TELEDETEKCJA ŚRODOWISKA
dawniej „Fotointerpretacja w geografii"
Tom 57 (2017/2) s. 27–34
ISSN 0071-8076
POLSKIE TOWARZYSTWO GEOGRAFICZNE
ODDZIAŁ TELEDETEKCJI I GEOINFORMATYKI
http://ptgeo.org.pl/teledetekcja/

Analysis of the suitability of selected image types in a texture analysis of satellite imagery

Przydatność wybranych typów obrazów w analizie tekstury zdjęć satelitarnych

Przemysław KUPIDURA
Katarzyna STANIAK

Politechnika Warszawska, Wydział Geodezji i Kartografii
Zakład Fotogrametrii, Teledetekcji i Systemów Informacji Przestrzennej
Pl. Politechniki 1
00-661 Warszawa
przemyslaw.kupidura@pw.edu.pl
kstaniak11@gmail.com

Abstract

The article presents studies on the impact of the source image type on the efficacy of image texture analysis in the terms of distinguishing classes of land use or land cover (LULC). Single gray-scale images are usually the inputs for this type of operation, however their selection is not unambiguous, especially in the case of multispectral images. Two very high resolution satellite images were used in the study: Pleiades (GSD: 2 m) and QuickBird (2.4 m). Five different input images were tested: the original near-infrared and red bands, the images of the first two main components, and the image of the normalised difference vegetation index – NDVI. Five LULC classes were compared to each other: bare soil, low vegetation, deciduous forests, coniferous forests and built-up areas. Granulometric analysis, as the one of the high efficient methods of texture analysis, was used for the test. Research results have shown that the choice of source image for this kind of processing can be very important for the efficacy of distinguishing between different LULC classes. NDVI images, and also the near infrared band and the first principal component were found most useful.

Streszczenie

Artykuł przedstawia badania dotyczące wpływu typu obrazu źródłowego na skuteczność analizy teksturowej obrazu z punktu widzenia wyodrębniania klas użytkowania lub pokrycia terenu (LULC). Tego typu operacjom poddawane są zazwyczaj pojedyncze obrazy w skali szarości, jednak ich wybór nie jest jednoznaczny, zwłaszcza w przypadku obrazów wielospektralnych. W badaniach wykorzystano dwa obrazy satelitarne o bardzo wysokiej rozdzielczości: Pleiades (GSD: 2 m) oraz QuickBird (2,4 m). Testowano pięć różnych obrazów wejściowych: oryginalne kanały bliskiej podczerwieni oraz czerwieni, obrazy dwóch pierwszych składowych głównych oraz obraz wskaźnika NDVI. Porównano wzajemnie pięć klas użytkowania lub pokrycia terenu: odkrytą glebę, niską roślinność, lasy liściaste, lasy iglaste oraz tereny zabudowane. Jako narzędzie testów wybrano analizę granulometryczną, jedną z metod analizy teksturowej o wysokiej skuteczności. Wyniki badań pokazały, że wybór obrazu źródłowego do przetworzeń może mieć bardzo duże znaczenie przy rozróżnianiu różnych klas użytkowania lub pokrycia terenu. Największą przydatnością cechowały się obrazy NDVI oraz kanału bliskiej podczerwieni i pierwszej składowej głównej.

Keywords: remote sensing, texture analysis, granulometric analysis, mathematical morphology, land cover classification.

Słowa kluczowe: teledetekcja, analiza teksturowa, analiza granulometryczna, morfologia matematyczna, klasyfikacja pokrycia terenu.

Introduction

Texture analysis is one of the important issues in satellite image processing. The texture is an important spatial feature of objects, allowing to distinguish different types of land use or land cover (LULC). The potential of texture analysis is especially high in combination with spectral analysis. The following studies show the effectiveness of such a spectro-texture approach to image analysis, mainly used in the classification of satellite images: Darling, Joseph (1968), Haralick *et al.* (1973), Weszka *et al.* (1976), Conners and Harlow (1980), Lam (1990), Mering and Chopin (2002), Bekkari *et al.* (2012), Wawrzaszek *et al.* (2013), Kupidura (2015), Kupidura and Skulimowska (2015).

The studies presented above are based on various methods of texture analysis. The texture has no unambiguous mathematical definition, therefore, there are various methods describing its various aspects. We can mention Gray Level Co-occurence Matrix – GLCM (Julesz 1962, Haralick *et al.* 1973), fractal analysis (Lam 1990), discrete wavelet transformation (Mallat 1989), Markov Random Fields (Spitzer 1971, Preston 1974) and granulometric analysis (Haas *et al.* 1967, Dougherty *et al.* 1992).

For the most part, the research focuses on the assessment of selected methods of texture analysis, possibly on the impact of spatial resolution of the image on the effectiveness of spectral-texture classification.

In this article we want to present research on the choice of source image. The operations used in texture analysis are based on individual images, e.g. binary or grayscale images. But, especially in the case of multispectral images, the choice of source image for processing is not straightforward. It can be one of the spectral images, it can be one of the result images of the main components analysis, it can also be images presenting various indices, e.g. vegetation indices.

This topic is not well researched, so it may be important to answer the question whether and how the choice of such an image may be important for the effectiveness of texture analysis.

Five different images of this type were tested: 2 images of spectral bands (red and near infrared), 2 images of the main components (1 and 2) and an image of the normalised difference vegetation index (NDVI). The source images were 2 multispectral very high resolution satellite images: Pleiades (GSD: 2 m) and QuickBird (GSD: 2.4 m). Earlier studies (Kupidura 2015, Kupidura *et al.* 2015a) showed that texture in images with such spatial resolution can be a very important feature that allows to distinguish selected classes of LULC.

Granulometric analysis was chosen as the method of texture analysis. It is a method of high efficiency, and, in addition, its multi-scality enables to easily analyze the significance of textures of different scales – different texture grain sizes. One can assume that the conclusions drawn on the basis of the results obtained can be extended to other methods of texture analysis. The methods differ from each other, but they are based on a common general principle: analyzing differences between adjacent pixels.

Methods and data

The analysis was based on 2 multispectral VHR images: Pleiades and Quickbird-2. Based on them, 5 types of single-layer images were generated, processed using texture granulometric analysis. Then, subsets of images (test sites) representing selected classes of land use and land cover (LULC) were selected and the separability of pixel value sets in texture images was examined using the Jeffries-Matusita distance measure (J-M).

Data preparation

Two multispectral VHR images were used in the analysis. They are presented in Table 1.

Table 1. Source image parameters
Tabela 1. Parametry obrazów źródłowych

Satellite	Acquisition date	Spectral bands	Ground sample distance (GSD)
Pleiades-1	May 2012	blue, green, red, near infrared	2.0 m
Quickbird-2	May 2002	blue, green, red, near infrared	2.4 m

Based on the above-mentioned images (hereinafter referred to as source images), a set of single-layer (grayscale) images was generated, in the next step processed using texture analysis. Below is a list of images with justification for the selection:

– Near Infrared band (NIR) – the original band presenting radiometric values in the near infrared range; the image in this area is highly sensitive to the state of vegetation, moreover, shady areas obtain very low radiometric values; this makes the texture elements potentially very contrasting;
– red band (R) – original band presenting radiometric values in the red range; it is an image with potentially small variations in value (compared to e.g. NIR images); however, in the case of selected remote sensing sensors, especially the older ones, without the possibility of recording in the near infrared range, it may potentially be a substitute for this channel;

– image of the first principal component (PC1) – image presenting values of the first component, generated on the basis of principal component analysis of the entire multispectral image; it is the image with the highest, by definition, variance (of all the images that can be generated within a given set of images), so the texture can potentially be the clearest;
– image of the second principal component (PC2) – image presenting values of the second principal component, generated on the basis of principal component analysis of the entire multispectral image; the image of the second principal component is, by definition, less variance than the image of the first component, however, the pixel diversity often shows the state of vegetation (the image of the second component is often referred to as "greenness"), which can cause a large variety of texture elements based on vegetation diversity;
– normalized differential vegetation index image (NDVI) – image showing the NDVI values calculated on the basis of NIR and R bands; as with the PC2 image, vegetation indices can well differentiate texture elements based on vegetation diversity; NDVI is one of the most popular and most commonly used vegetation indices.

As a result, 10 images were created – 5 for each of the two multispectral images – which formed the basis for further analysis. They were subjected to texture analysis using the granulometric approach. Hereinafter these images will be called test images.

Brief presentation of granulometric analysis

Granulometric analysis is one of many image processing methods that can be used for image texture analysis. In its classical form, it involves performing a sequence of opening operations (Haas *et al*. 1967) of a morphological binary image with the sequentially increasing size of the structuring element. Then, the number of individual differential images is calculated (in the case of binary images it is the number of pixels with a value of 1), which means the number of texture elements of the appropriate size in the analyzed image. Similarly, granulometry based on the closing operation is also performed. In this situation, the information obtained relates to dark texture elements (just like opening-based granulometry provides information about bright elements). In the case of grayscale images, the granulometric processing is analogous, except that the image size means the sum of all pixel values.

For classification purposes, local granulometric analysis (Dougherty *et al*. 1992, Vincent 1996), which in-volves performing the above-described processing separately for each pixel in its appropriately defined neighborhood, may be useful. In this way, each pixel is assigned values that determine the nature of the texture in its neighbourhood.

Granulometric analysis is characterized by several important features that distinguish it from other methods. These are primarily multi-scale (information applies to texture elements of different sizes) and resistance to edge effects (Ruiz *et al*. 2004).

The efficacy of this method is shown in previous studies (Merring, Chopin 2002, Kupidura *et al*. 2010, Kupidura 2015, Kupidura *et al*. 2015b).

Methodology

Each type of test image generated on the basis of each of the two source images was subjected to granulometric analysis based on opening and closing using structuring elements in pseudo-circular shapes of sizes from 1 to 3 pixels. As a result, for each test image obtained on the basis of each source image, 6 granulometric maps were obtained: 3 for opening and 3 for closing. In total, 60 granulometric maps (30 for each source image) were obtained. Their list, together with the symbols used later in this article, is presented in Table 2.

Table 2. Test images; *pl* or *qb* indicate the source image (Pleiades or QuickBird), *nir*, *ndvi* etc. mean test image type, *o1* and *c2* – opening or closing operation and the size of structuring element

Tabela 2. Obrazy testowe; pl *lub* qb *oznacza obraz źródłowy (Pleiades lub QuickBird),* nir, ndvi *itd. oznacza rodzaj obrazu testowego,* o1 *lub* c2 *– otwarcie lub domknięcie oraz rozmiar elementu strukturującego*

				Type of granulometry					
				Opening			Closing		
				Size of structuring element / No. of granulometric map					
				1	2	3	1	2	3
Source image	Pleiades	Test image	NIR	pl-nir-o1	pl-nir-o2	pl-nir-o3	pl-nir-c1	pl-nir-c2	pl-nir-c3
			R	pl-r-o1	pl-r-o2	pl-r-o3	pl-r-c1	pl-r-c2	pl-r-c3
			NDVI	pl-ndvi-o1	pl-ndvi-o2	pl-ndvi-o3	pl-ndvi-c1	pl-ndvi-c2	pl-ndvi-c3
			PC1	pl-pc1-o1	pl-pc1-o2	pl-pc1-o3	pl-pc1-c1	pl-pc1-c2	pl-pc1-c3
			PC2	pl-pc2-o1	pl-pc2-o2	pl-pc2-o3	pl-pc2-c1	pl-pc2-c2	pl-pc2-c3
	QuickBird		NIR	qb-nir-o1	qb-nir-o2	qb-nir-o3	qb-nir-c1	qb-nir-c2	qb-nir-c3
			R	qb-r-o1	qb-r-o2	qb-r-o3	qb-r-c1	qb-r-c2	qb-r-c3
			NDVI	qb-ndvi-o1	qb-ndvi-o2	qb-ndvi-o3	qb-ndvi-c1	qb-ndvi-c2	qb-ndvi-c3
			PC1	qb-pc1-o1	qb-pc1-o2	qb-pc1-o3	qb-pc1-c1	qb-pc1-c2	qb-pc1-c3
			PC2	qb-pc2-o1	qb-pc2-o2	qb-pc2-o3	qb-pc2-c1	qb-pc2-c2	qb-pc2-c3

For the purposes of texture analysis, 5 LULC classes with different textures were selected:
– bare sol,
– low vegetation,
– coniferous forest,
– deciduous forest,
– built-up areas.

The first two classes: bare soil and low vegetation, have low texture, while the other three classes: wooded and built-up areas have relatively high texture, with varying degrees of its intensity, especially on very high resolution images. Three test fields were prepared for each class (on each of the source images). They are shown below in Fig. 1.

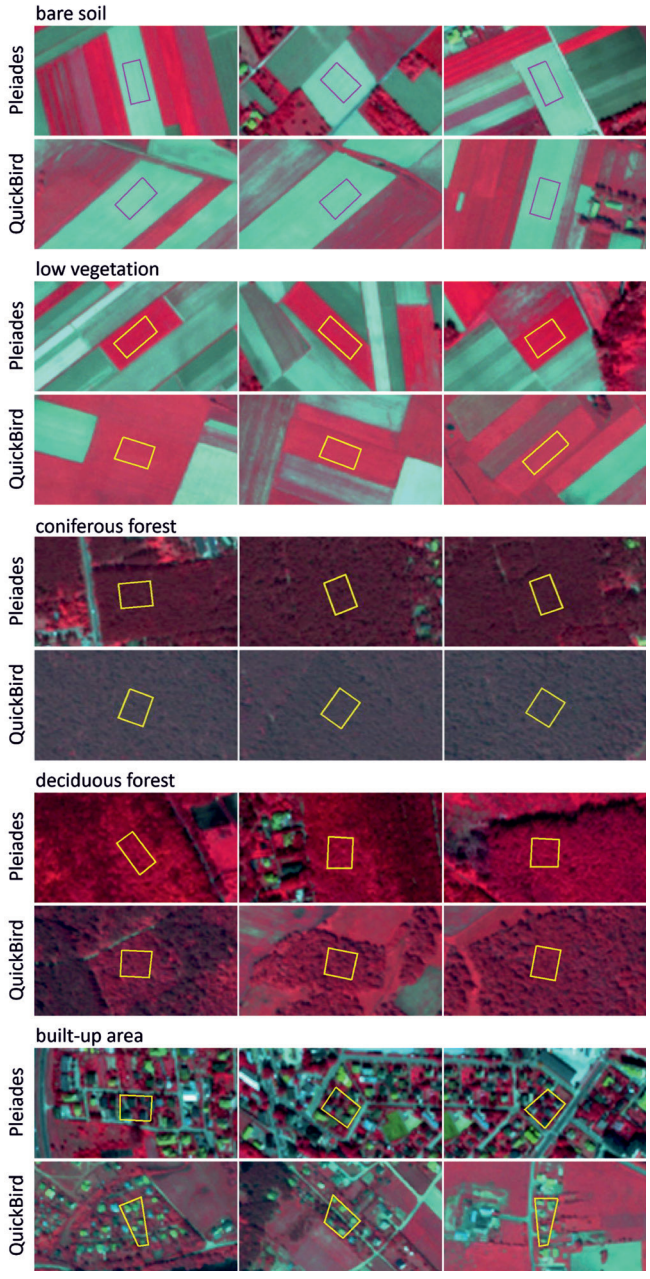

Fig. 1. Test sites representing individual classes in both source images in the RGB 432 composition

Ryc. 1. Pola testowe reprezentujące poszczególne klasy na obydwu obrazach źródłowych w kompozycji RGB 432

The assessment of the usefulness of individual types of test images was based on an analysis of the separability of pixel values from test fields representing individual classes of LULC. Separability was assessed using the Jeffries-Matusita distance. It is calculated according to the following formula (Swain, Davis 1978):

$$JM_{ij} = \sqrt{2(1 - e^{-a})}$$

where a is a Bhattacharya distance:

$$a = \frac{1}{8}(\mu_i - \mu_j)^T \left(\frac{C_i - C_j}{2}\right)(\mu_i - \mu_j) + \frac{1}{2}\ln\left(\frac{(|(C_i + C_j)/2|)}{\sqrt{|C_i| \times |C_j|}}\right)$$

gdzie:
i, j – two compared pixel groups,
C_i – covariance matrix for group i,
C_j – covariance matrix for group j,
μ_i – mean vector for group i,
μ_j – mean vector for group j,
$|C_i|$ – matrix determinant C_i,
$|C_j|$ – matrix determinant C_j.

The Jeffries-Matusita distance calculated according to the above formula takes values from 0 to $\sqrt{2}$ (approximately 1.414). A value of $\sqrt{2}$ means that the compared pixel groups are fully separable. The following degrees of distinguishability of pairs of land cover classes were adopted in the research:
– low separability: from 0 to 0,999,
– moderate separability: from 1 to 1,299,
– very good separability: from 1,3 to 1,414.

The test consisted in comparing the values of pixels on individual granulometric maps (presented in Table 2) between all pairs of LULC classes and calculating their separability. The comparisons were carried out within one source image (Pleiades or QuickBird). For example, in the Pleiades picture, a comparison of two classes (e.g. low vegetation and built-up area) consisted of performing nine J-M distance tests on one granulometric map.

The separability of values in spectral images was not analyzed.

Results and discussion

Considering the number of compared test field pairs, a large number of J-M distance analysis results were obtained on all granulometric maps based on test images from two source images: 5400. Five test images were selected for each of the two source images; 6 granulometric maps were created on each of the test images, were the separability of 10 pairs of land cover classes was analyzed; each class was represented by 3 test fields, which gave 9 pairs of test fields. In order to simplify the presentation of results, the values obtained for individual pairs of test fields have been aggregated. Analysis of the obtained values showed that the median value is the most representative value. Table 3 shows the median values obtained for individual pairs of LULC classes (for all test sites), depending on the type of granulometric map, test image and source image.

Table 3. Median J-M values obtained for individual pairs of classes, depending on the source image, test image and type of granulometric map

Tabela 3. Mediany wartości J-M uzyskane dla poszczególnych par klas, w zależności od obrazu źródłowego, testowego i rodzaju mapy granulometrycznej

			Pair of LULC classes									
			soil-con. forest	soil-dec. forest	soil-built-up	con. forest-low veg.	dec. forest-low veg.	low veg.-built-up	con. forest-dec. forest	con. forest-built-up	dec. forest-built-up	soil-low veg.
1	2	3	4	5	6	7	8	9	10	11	12	13
Source image	Test image	Gran. map	J-M median values									
Pleiades	NIR	pl_nir_o1	1,414	1,414	1,414	1,414	1,414	1,414	1,413	1,405	0,564	1,323
		pl_nir_o2	1,414	1,413	1,414	1,363	1,405	1,402	1,337	1,369	0,835	1,310
		pl_nir_o3	1,390	1,411	1,411	0,742	1,386	1,386	1,336	1,371	0,969	1,331
		pl_nir_c1	1,414	1,414	1,414	1,414	1,414	1,413	1,387	1,210	0,657	1,020
		pl_nir_c2	1,408	1,414	1,413	1,288	1,411	1,409	1,297	1,364	0,831	1,230
		pl_nir_c3	1,351	1,414	1,414	0,804	1,390	1,414	1,345	1,410	1,363	1,230
	R	pl_r_o1	0,469	0,503	1,411	1,225	1,374	1,413	0,684	1,410	1,410	1,092
		pl_r_o2	0,485	0,455	1,392	1,118	1,004	1,404	0,617	1,392	1,397	1,041
		pl_r_o3	0,619	0,395	1,411	0,534	0,507	1,412	0,621	1,413	1,411	0,469
		pl_r_c1	0,570	0,552	1,397	1,138	1,141	1,409	0,458	1,399	1,394	0,750
		pl_r_c2	0,411	0,514	1,412	0,774	0,922	1,413	0,505	1,410	1,408	0,836
		pl_r_c3	0,887	0,583	1,407	0,760	0,741	1,408	0,921	1,412	1,404	0,435
	NDVI	pl_ndvi_o1	1,414	1,414	1,414	1,414	1,414	1,414	1,414	1,411	1,414	0,569
		pl_ndvi_o2	1,414	1,382	1,414	1,414	1,367	1,414	1,268	1,412	1,414	0,499
		pl_ndvi_o3	1,411	1,364	1,414	1,382	1,328	1,414	0,940	1,410	1,413	0,721
		pl_ndvi_c1	1,414	1,414	1,414	1,414	1,413	1,414	1,376	1,246	1,412	0,619
		pl_ndvi_c2	1,414	1,408	1,414	1,414	1,399	1,414	1,141	1,394	1,413	0,515
		pl_ndvi_c3	1,408	1,381	1,414	1,348	1,030	1,414	1,193	1,414	1,414	0,939
	PC1	pl_pc1_o1	1,414	1,414	1,414	1,414	1,414	1,414	1,411	1,403	0,727	1,316
		pl_pc1_o2	1,414	1,411	1,410	1,367	1,403	1,405	1,282	1,369	0,807	1,277
		pl_pc1_o3	1,390	1,406	1,410	1,090	1,372	1,397	1,260	1,378	0,967	1,230
		pl_pc1_c1	1,414	1,414	1,414	1,414	1,414	1,414	1,384	1,351	0,412	0,942
		pl_pc1_c2	1,394	1,412	1,414	1,312	1,406	1,413	1,266	1,392	0,905	0,832
		pl_pc1_c3	1,284	1,414	1,414	0,841	1,401	1,414	1,320	1,409	1,364	0,796
	PC2	pl_pc2_o1	0,514	1,154	1,405	0,871	1,375	1,407	1,137	1,397	1,385	0,524
		pl_pc2_o2	0,707	1,350	1,412	1,068	1,214	1,412	1,338	1,409	1,406	0,543
		pl_pc2_o3	0,535	0,911	1,413	0,664	0,399	1,412	1,110	1,413	1,410	0,618
		pl_pc2_c1	0,832	1,285	1,411	0,975	1,402	1,413	1,195	1,410	1,397	0,521
		pl_pc2_c2	0,714	1,293	1,409	0,668	1,167	1,406	1,281	1,407	1,379	0,786
		pl_pc2_c3	0,484	1,234	1,413	0,798	0,700	1,412	1,240	1,413	1,410	0,740

Table 3. (continued)
Tabela 3. (cd.)

1	2	3	4	5	6	7	8	9	10	11	12	13
QuickBird	NIR	qb_nir_o1	1,414	1,414	1,414	1,414	1,414	1,414	1,414	1,393	0,653	1,395
		qb_nir_o2	1,414	1,414	1,414	1,410	1,414	1,414	1,412	1,411	0,978	1,127
		qb_nir_o3	1,413	1,414	1,412	1,246	1,405	1,408	1,369	1,401	0,765	1,237
		qb_nir_c1	1,414	1,414	1,414	1,414	1,414	1,414	1,410	1,413	0,535	1,400
		qb_nir_c2	1,413	1,414	1,414	1,358	1,414	1,414	1,395	1,411	0,906	1,162
		qb_nir_c3	1,327	1,404	1,411	0,690	1,388	1,406	1,254	1,399	1,252	1,010
	R	qb_r_o1	1,390	1,182	1,414	1,301	1,087	1,414	0,540	1,414	1,414	0,819
		qb_r_o2	0,523	0,433	1,405	0,839	0,950	1,410	0,379	1,405	1,406	0,916
		qb_r_o3	0,765	0,801	1,390	0,513	0,598	1,382	0,470	1,377	1,357	0,340
		qb_r_c1	1,303	1,058	1,411	1,378	1,265	1,412	0,640	1,398	1,405	0,586
		qb_r_c2	1,238	1,204	1,413	1,361	1,317	1,413	0,326	1,409	1,409	0,904
		qb_r_c3	0,896	0,787	1,413	1,031	0,865	1,413	0,361	1,411	1,411	0,788
	NDVI	qb_ndvi_o1	1,414	1,414	1,414	1,414	1,414	1,414	0,514	1,374	1,387	0,629
		qb_ndvi_o2	1,414	1,413	1,414	1,414	1,412	1,414	0,808	1,414	1,411	0,571
		qb_ndvi_o3	1,402	1,409	1,414	1,376	1,406	1,414	1,008	1,413	1,409	0,703
		qb_ndvi_c1	1,414	1,414	1,414	1,414	1,414	1,414	0,669	1,400	1,374	0,502
		qb_ndvi_c2	1,414	1,410	1,414	1,411	1,395	1,414	0,499	1,413	1,412	0,967
		qb_ndvi_c3	1,410	1,398	1,412	1,391	1,376	1,411	0,687	1,407	1,399	0,519
	PC1	qb_pc1_o1	1,414	1,414	1,414	1,414	1,414	1,414	1,414	1,357	0,638	1,291
		qb_pc1_o2	1,414	1,414	1,414	1,408	1,414	1,414	1,410	1,410	0,907	1,062
		qb_pc1_o3	1,407	1,408	1,410	1,278	1,394	1,406	1,313	1,393	0,648	1,095
		qb_pc1_c1	1,414	1,414	1,414	1,414	1,414	1,414	1,401	1,413	0,731	1,314
		qb_pc1_c2	1,409	1,414	1,414	1,380	1,414	1,414	1,346	1,402	0,851	0,778
		qb_pc1_c3	1,109	1,404	1,405	0,618	1,347	1,391	1,322	1,385	1,029	0,680
	PC2	qb_pc2_o1	1,414	1,414	1,414	1,145	1,414	1,414	1,414	1,357	1,361	1,161
		qb_pc2_o2	1,279	1,412	1,414	0,863	1,383	1,414	1,370	1,357	1,398	0,806
		qb_pc2_o3	0,408	1,290	1,410	0,489	1,160	1,404	1,218	1,408	1,381	0,483
		qb_pc2_c1	1,374	1,414	1,414	1,270	1,414	1,414	1,413	1,357	1,320	0,983
		qb_pc2_c2	1,065	1,414	1,414	0,568	1,411	1,414	1,381	1,357	1,408	0,844
		qb_pc2_c3	0,652	1,411	1,414	0,632	1,405	1,414	1,403	1,414	1,406	0,735

In Table 3, for better readability, result values in different ranges are marked with different colors. Green means very good separability of the analyzed classes. Yellow means moderately good separability. And pink means low separability of the analyzed pair of LULC classes.

Comparison of the two parts of the table for both source images (Pleiades and QuickBird) shows a significant similarity of the results obtained for them. Therefore, the analysis of results below will apply to both source images.

First of all, it should be noted that the choice of test image can be important. Also, it is definitely easier to point out the worst test images among analyzed. These are images of the red band (R) and the second principal component (PC2). But even in their case, it is possible to indicate pairs of classes whose separability on granulometric maps developed on the basis of these images is good – these are pairs in which one of the compared classes is built-up area. This is due to the very strong texture of built-up areas, also evident in R and PC2 images. It is worth noting that these class pairs (with built-up areas) stand out very well on almost all (with exceptions) test images, also on most of the analyzed granulometric maps. However, the distinction between other class pairs is much less clear in these two test images.

It is more difficult to point to the best test image.

Analyzing the remaining 3 images: near infrared (NIR), vegetation index (NDVI) and the first principal component (PC1) one can notice a large similarity of the results obtained for the NIR and PC1 images, and a bit

different results obtained for the NDVI image. For all these 3 types of images, good results were obtained for most of the analyzed class pairs. However, it is worth noting some differences between these images. First of all, granulometric maps developed on the basis of the NDVI image give a weak distinction between types of forest: deciduous and coniferous, while NIR and PC1 images give good results in this respect. In turn, NDVI gives a very good distinction between the classes of deciduous forest and built-up areas, while NIR and PC1 images are of little use in this respect.

The case of poor forest discrimination in NDVI images should be explained by the relatively strong texture of these cover classes in the vegetation indicator image. For both deciduous and coniferous forests, a large (and similar) difference can be observed between the shaded and illuminated parts of the tree crowns, which results in similar values on granulometric maps. However, it should be emphasized that the texture in these cases is not very high, which is due to the normalization used in the NDVI indicator, which causes some brightening of the darker fragments of the tree crowns. In contrast, in NIR and PC1 images the difference in brightness between these areas is more important – while the shaded areas are similarly dark in both types of forests, the illuminated fragments of deciduous tree crowns are much brighter in both the NIR and PC1 images. And this translates into higher values on granulometric maps, and as a result, into good separability.

It should be noted that the principal components analysis was based on 4 spectral bands. For a different number of spectral bands, i.e. when using systems with better spectral resolution, the results for this type of image may be different.

Also in the case of the pair: deciduous forest – built-up areas, the usefulness of these three analyzed source images is different. Better separability was obtained on the basis of NDVI images, because in built-up areas a very high texture can be observed, due to the large variety of types of land cover (both vegetation and non-vegetation ones) that make up this class – in the case of deciduous forest image, the texture, although clear, is less visible, as we mentioned earlier.

All source images show little or very little utility when it comes to distinguishing between uncovered soil and low vegetation. This result is in line with expectations – both classes are characterized by very low texture, what results in similarly low values on subsequent granulometric maps. Here, however, it should be emphasized that texture analysis is not so important when it comes to distinguishing between these two classes – they are relatively homogeneous and very different in terms of spectral values. Therefore, spectral analysis is sufficient for these two LULC classes.

Analysis of the results shows that in the case of the tested images, grain size maps with the lowest indexes, which define the texture with the smallest grain size, are slightly more useful. However, no unequivocal trend was observed in the types of granulometric maps due to the operations: opening or closing.

Fig. 2 presents sample test sites on granulometric maps created on the basis of the Pleiades image.

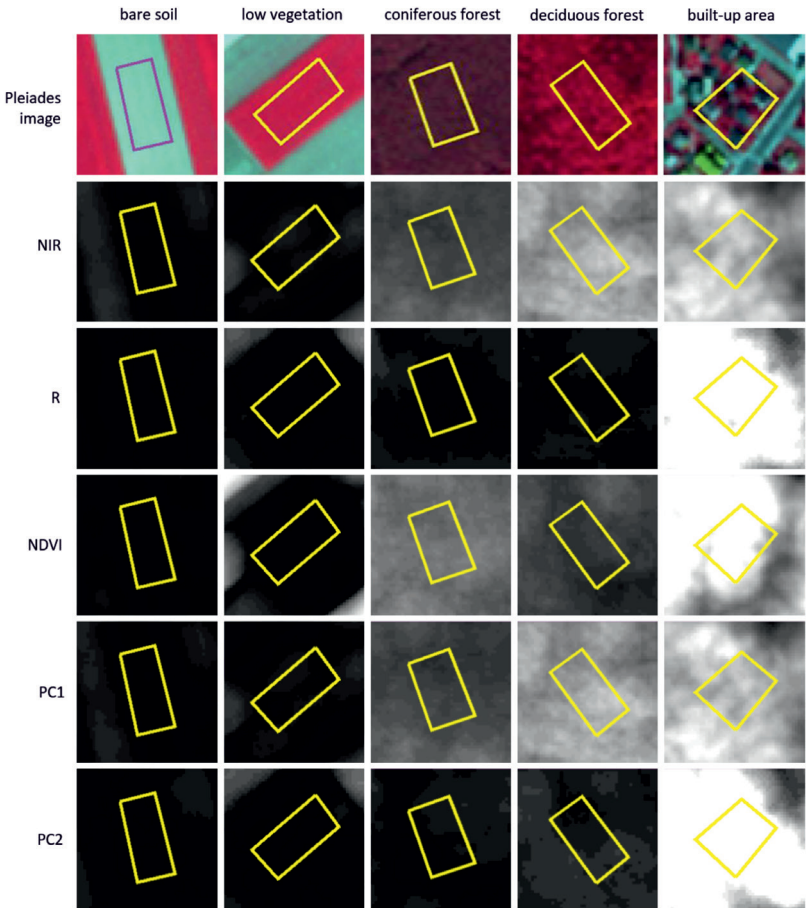

Fig. 2. Test sites representing individual classes in the RGB 432 composition (Pleiades image) and in the granulometric maps (opening, structuring element size: 1) created basing on different test images

Ryc. 2. Pola testowe reprezentujące poszczególne klasy na kompozycji RGB 432 (obraz Pleiades) oraz na mapach granulometrycznych (otwarcie, rozmiar elementu strukturującego: 1) utworzonych na podstawie poszczególnych obrazów testowych

Conclusions

The presented research results show that the choice of image on the basis of which texture analysis is performed can be of great importance. The best results were obtained for NDVI images and near infrared band (NIR) and the first principal component (PC1). Images of red band (R) and the second principal component turned out to be clearly worse in this set. At the same time, it should be emphasized that the images for which the best results were obtained did not give equally good results for the same pairs of compared LULC classes. This indicates that the texture of different classes of land cover can manifest themselves in these images to a greater or lesser extent. It follows that one can consider the appropriate selection of images for conducting texture analysis depending on the target classes of LULC.

To conduct texture analysis, granulometric approach was used. However, the conclusions obtained from the research can also be extended to other methods of texture analysis. It can be expected that the obtained separability may be different for other methods, but similar trends can be expected when it comes to the usefulness of particular types of images.

Bibliography

Bekkari A., Idbraim S., Elhassouny A., Mammass D., El Yassa M., Ducrot D., 2012, SVM and Haralick Features for Classification of High Resolution Satellite Images from Urban Areas, [in:] Elmoataz A., Mammass D., Lezoray O., Nouboud F., Aboutajdine D. (Eds.), ICISP 2012, Springer, Berlin/Heidelberg, Germany, 17–26.

Conners R.W., Harlow C.A., 1980, A Theoretical Comaprison of Texture Algorithms, IEEE Trans. Pattern Anal. Mach. Intell 2, 204–222.

Darling E.M., Joseph R.D., 1968, Pattern recognition from satellites altitudes, IEEE Trans. Syst. Man Cybern. 4, 30–47.

Dougherty E.R., Pelz J.B., Sand F., Lent A., 1992, Morphological Image Segmentation by Local Granulometric Size Distributions, Journal of Electronic Imaging 1(1), 46–60.

Haas A., Matheron G., Serra J., 1967, Morphologie Mathématique et granulométries en place, Annales des Mines 12, 768–782.

Haralick R.M., Shanmugam K., Dinstein I., 1973, Textural Features for Image Classification, IEEE Trans. Syst. Man Cybern 4, 610–621.

Julesz B., 1962, Visual pattern discrimination, IRE Transactions on Information Theory 8(2), 84–92.

Kupidura P., Koza P., Marciniak J., 2010, Morfologia matematyczna w teledetekcji, Wydawnictwo Naukowe PWN, Warszawa, 1–250.

Kupidura P., 2015, Wykorzystanie granulometrii obrazowej w klasyfikacji treści zdjęć satelitarnych, Prace Naukowe Politechniki Warszawskiej, Warsaw University of Technology Publishing House.

Kupidura P., Skulimowska M., 2015, Morphological profile and granulometric maps in extraction of buildings in VHR satellite images, Archives of Photogrammetry, Cartography and Remote Sensing 27, 83–96.

Kupidura P., Kłębowski M., Ściana P., Truszkiewicz P., 2015a, Analiza możliwości rozróżniania wybranych klas pokrycia terenu na zdjęciach satelitarnych z wykorzystaniem granulometrii obrazowej, [in:] Dzięgielewski A., Szychowski D., Wernik J. (Eds.), Wybrane problemy techniki, 53–63.

Kupidura P., Popławski W., Sitko P., 2015b, Comparison of efficiency of extraction of built-up areas in aerial images using fractal analysis and morphological granulometry, Teledetekcja Środowiska 52(1), 29–37.

Lam N.S.N., 1990, Description and Measurement of Landsat TM Using Fractals, Photogramm. Eng. Remote Sens 56, 187–195.

Mallat S.G., 1989, A Theory for Multiresolution Signal Decomposition: The Wavelet Representation, IEEE Transactions on Pattern Analysis and Machine Intelligence 11(7), 674–693.

Mering C., Chopin F., 2002, Granulometric maps from high resolution satellite images, Image Anal. Stereol 21, 19–24.

Preston C.J., 1974, Gibbs States on Countable Sets, Cambridge University Press.

Ruiz L.A., Fdez-Sarria A., Recio J.A., 2004, Texture feature extraction for classification of remote sensing data using wavelet decomposition: a comparative study, International Archives of Photogrammetry and Remote Sensing 35.

Spitzer F., 1971, Random fields and interacting particle systems, M.A.A. Summer Seminar Notes.

Swain P.H., Davis S.M., 1978, Remote Sensing. The Quantitative Approach, Megraw-Hill College, 1–396.

Vincent L., 1996, Opening Trees and Local Granulometries, [in:] Proc. Mathematical Morphology and Its Applications to Signal Processing, Georgia, USA, 273–280.

Wawrzaszek A., Krupiński M., Aleksandrowicz S., Drzewiecki W., 2013, Fractal and multifractal characteristics of very high resolution satellite images, [in:] Proceedings of the 2013 IEEE International Geoscience and Remote Sensing Symposium – IGARSS, Melbourne, VIC, Australia, 21–26 July 2013, 1501–1504.

Weszka J.S., Dyer C.R., Rosenfeld A., 1976, A Comparative Study of Texture Measures for Terrain Classification, IEEE Trans. Syst. Man Cybern 6, 269–285.

Przemysław Kupidura, Katarzyna Staniak
Teledetekcja Środowiska
Polskie Towarzystwo Geograficzne
Oddział Teledetekcji i Geoinformatyki – Warszawa 2017